Separation of the Geodetic Consequences of Past and Present Ice-Mass Change: Influence of Topography with Application to Svalbard (Norway)

A. Mémin,[1] J. Hinderer,[1] and Y. Rogister[1]

Abstract—Polar regions such as Greenland, Svalbard and Antarctica are deforming today because of both the present-day ice-mass (PDIM) change of glaciers and the glacial isostatic adjustment (GIA) following the Pleistocene deglaciation. Observations handled in these areas contain both the contributions from the PDIM change and GIA. This study aims at separating them by considering two specific gravity variation-to-vertical displacement ratios. We first review the case of the viscoelastic rebound (GIA) subsequent to the Pleistocene deglaciation leading to a ratio C^v. The outcome of previous studies is that C^v is approximately equal to $-0.15 \, \mu$Gal/mm and almost independent of the deglaciation history, ice geometry and viscosity profile of the mantle. Similarly we consider the elastic deformation resulting from PDIM change which leads to a second ratio $C^{e,N}$. Several studies have shown that $C^{e,N} \approx -0.26 \, \mu$Gal/mm if one assumes that the changing glaciers are thin layers over the surface of a spherical Earth model. In this case, we show that the separation between the contributions from PDIM change and GIA is unique if both gravity and height changes observations are available at the same station. Next, we focus on $C^{e,N}$ and show that according to the deglaciation/glaciation context and from colocated gravity variation and ground vertical velocity measurements one can deduce a range of possible values for $C^{e,N}$. Studying the influence of the topography on $C^{e,N}$ we first show that it tends to positive values if most of surrounding ice-mass changes above the altitude of the observation site and to values lower than $-0.26 \, \mu$Gal/mm if changes are below. We next apply our general formalism to the case of the past and PDIM changes in Svalbard, Norway. We compute the ratio $C^{e,N}$ at the geodetic observatory at Ny-Ålesund and show the influence of the topography of the surrounding glaciers on the measured gravity and uplift rates. We show that if the ice-mass change is spatially uniform, $C^{e,N}$ does not depend on the speed of ice-mass change, and hence the separation of the contributions from PDIM changes and GIA can still be done univocally. However, if the ice-mass change is not spatially uniform, $C^{e,N}$ depends on both the speed of ice-mass change and the volume of ice-change rate.

Key words: Gravity variation-to-vertical displacement ratio, present-day ice thinning, glacial isostatic adjustment, topography, Svalbard.

[1] IPGS/UMR 7516, Université de Strasbourg/EOST, CNRS, 5 rue René Descartes, 67084 Strasbourg Cedex, France. E-mail: anthony.memin@unistra.fr

1. Introduction

In response to climatic changes, ice-masses vary. Currently a reduction of the volume of ice is observed using different methods. For example, the analysis of space gravimetric observations from GRACE (Gravity Recovery and Climate Experiment) suggests ice-mass loss over Alaska (e.g. Luthcke *et al.* 2008), Greenland and West Antarctica (e.g. Barletta *et al.* 2008; Wouters *et al.* 2008; Slobbe *et al.* 2009; Horwath and Dietrich 2009; Velicogna 2009). Comparison of digital elevation models deduced from satellite altimetry or photogrammetry have shown ice thinning in Svalbard (e.g. Kohler *et al.* 2007; Kääb 2008; Nuth *et al.* 2010). Ice thinning has also been shown in Alaska by using satellite imagery (Berthier *et al.* 2010).

The solid Earth elastically deforms because of this present-day ice-mass (PDIM) change. Moreover, most of the regions where the ice-mass presently decreases is also subject to the glacial isostatic adjustment (GIA), which is the viscous relaxation that follows the Pleistocene deglaciation. Of course, the observations (ground gravimetry and precise positioning) do not separate the two effects (e.g. Bevis *et al.* 2010). Usually, models of deglaciation histories are used to compute the GIA, which is subtracted from the observations. The volume of ice loss can then be deduced from the residuals. The contribution of the GIA to the observations is sometimes estimated using the vertical displacement to gravity conversion factor of Wahr *et al.* (1995). It appears difficult to separate the two contributions by using observations only.

We study the separation between the contributions from past and present deglaciations to the observations by using two gravity variation-to-vertical displacement ratios, for both the viscous (C^v) and

elastic ($C^{e,N}$) deformations. In Sect. 2, we first list the relations between the observed and theoretical vertical displacement and gravity rates. Then we collect ratios of gravity rate to vertical velocity found in the literature (Sects. 2.1 and 2.2) and relate them to the observed parameters (Sect. 2.3). In Sect. 3 we focus on $C^{e,N}$. We study the influence of the glaciation/deglaciation context (Sect. 3.1) and the effect of the topography, for which we derive a general expression (Sects. 3.2 and 3.3). We investigate in the last section the influence of the topography and spatial distributions of ice-mass variations on the separation of the geodetic consequences of past and present-day ice-mass change over the Svalbard archipelago, Norway (Sect. 4). After a brief geographical description of Svalbard in Sect. 4.1, we introduce, in Sect. 4.2, the spatial distribution of the glaciers and the different vertical profiles of ice-mass change used to model the gravity variations and ground velocity (Sect. 4.3). We discuss the results from models and observations in Sect. 4.4.

2. Viscoelastic and Elastic Gravity and Uplift Rates

Let δu^v and δg^v be respectively the time variations of the vertical displacement and gravity rate due to the GIA at the Earth's surface. The uplift and gravity rates induced by the PDIM change are respectively denoted by δu^e and $\delta g^e + \delta g^N$. The first term δg^e is due to the elastic deformation of the ground, the second term is the Newtonian attraction of the varying mass. In areas subject to both the GIA and PDIM change, the observed vertical velocity δu^{obs} and gravity rates δg^{obs} are given by

$$\delta u^{\mathrm{obs}} = \delta u^e + \delta u^v, \tag{1}$$

$$\delta g^{\mathrm{obs}} = \delta g^e + \delta g^N + \delta g^v. \tag{2}$$

2.1. Gravity Variation-to-Vertical Displacement Ratio for Viscoelastic Deformation

Using different deglaciation histories, ice geometries and viscosity profiles for the mantle of a viscoelastic Maxwell Earth, Wahr et al. (1995) found the following relation between the viscous gravity and uplift rates:

$$C^v = \frac{\delta g^v}{\delta u^v} \approx -0.15 \, \mu\mathrm{Gal/mm}. \tag{3}$$

This ratio was studied by Fang and Hager (2001) who confirmed that it is independent of the radial viscosity profile of the Earth, which is due to the nearly incompressible viscous response of a Maxwell Earth. Using the ICE-3G history of Tushingham and Peltier (1991) to model the GIA in Antarctica, James and Ivins (1998) numerically found a ratio of $-0.16 \, \mu\mathrm{Gal/mm}$, close to ratio (3). Actually, the viscous response of the Earth involves both changes in the height of the surface and mantle mass redistribution. The motion of the surface involves a variation of the gravity measured by an instrument moving with the surface. This variation is the so-called free-air gradient, which is $-2 \, g_0/a \approx -0.31 \, \mu\mathrm{Gal/mm}$, where a is the mean Earth radius and $g_0 = 9.81 \, \mathrm{m/s^2}$ is the surface gravity. The second effect can be approximated by the Bouguer plate formula leading to $2\pi G\rho_m$ for the gravity variation-to-vertical displacement ratio, where G is the gravitational constant and ρ_m is the density of the plate. Taking $\rho_m = 3{,}350$ $\mathrm{kg/m^3}$ as an average density for the upper mantle, we have $2\pi G \, \rho_m = 0.14 \, \mu\mathrm{Gal/mm}$ and $\delta g^v/\delta u^v \approx -0.17 \, \mu\mathrm{Gal/mm}$, as found for example in Ekman and Mäkinen (1996), James and Ivins (1998) and Le Meur and Huybrechts (2001). This ratio is close to the one first derived by Wahr et al. (1995), although it is derived from a simpler modeling.

The ratio $C^v = -0.15 \, \mu\mathrm{Gal/mm}$ given by Wahr et al. (1995) was also obtained by Larson and van Dam (2000) in North America from uplift and gravity observations, whereas Lambert et al. (2006) obtained $-0.18 \pm 0.03 \, \mu\mathrm{Gal/mm}$ from similar observations. In Fennoscandia, Mäkinen et al. (2005) obtained a ratio in the range $[-0.18 \pm 0.06, \, -0.16 \pm 0.04] \, \mu\mathrm{Gal/mm}$. Some studies (e.g. Wolf et al. 1997; Lambert et al. 2001; Mäkinen et al. 2007; Amalvict et al. 2009) used a ratio in the range $[-0.17, \, -0.15] \, \mu\mathrm{Gal/mm}$ to predict the gravity rate from a modelled displacement rate.

2.2. Gravity Variation-to-Vertical Displacement Ratio for Elastic Deformation

Using a spectral approach, de Linage et al. (2007) computed the ratio

$$C^e = \frac{\delta g^e}{\delta u^e} \qquad (4)$$

between the rates of gravity and vertical displacement for an elastic deformation. According to the compressibility of the uppermost layer of the Earth model, its value is either $\approx -0.20\,\mu\text{Gal/mm}$ if the layer is incompressible or $\approx -0.24\,\mu\text{Gal/mm}$ if it is compressible.

These values do not take into account the direct attraction of the changing mass expressed by δg^N. Considering that the mass changes occur at the surface of the spherical and compressible Earth model, de LINAGE *et al.* (2007) found that outside the area where the load occurs

$$C^{e,N} = C^e + C^N \approx -0.26\,\mu\text{Gal/mm}, \qquad (5)$$

where

$$C^N = \frac{\delta g^N}{\delta u^e}. \qquad (6)$$

They obtained this value by averaging over the harmonic degrees 2–50 the ratio between the *n*th spectral components of the transfer functions of the gravity variation and vertical displacement. For the harmonic degrees 6 and 3,000, this ratio takes the values -0.2881 and $-0.2467\,\mu\text{Gal/mm}$, respectively.

JAMES and IVINS (1998) obtained $C^{e,N} = -0.27$ $\mu\text{Gal/mm}$, which is close to the value (5) found by de LINAGE *et al.* (2007) and which corresponds to 85% of the free-air gradient. As for the viscous ratio, $C^{e,N}$ is used to estimate secular gravity variation from modelled uplift rate such as that due to the PDIM change in Antarctica (e.g. MÄKINEN *et al.* 2007; AMALVICT *et al.* 2009).

2.3. Separation Between the Geodetic Consequences of GIA and PDIM Change

For colocated gravimetric and geodetic stations, relations (1), (2), (3) and (5) provide

$$\delta u^e = \frac{\delta g^{\text{obs}} - C^v \delta u^{\text{obs}}}{C^{e,N} - C^v}, \qquad (7)$$

$$\delta u^v = -\frac{\delta g^{\text{obs}} - C^{e,N} \delta u^{\text{obs}}}{C^{e,N} - C^v}, \qquad (8)$$

which, in turn, give δg^v and $\delta g^e + \delta g^N$ by using (3) and (5):

$$\delta g^e + \delta g^N = C^{e,N} \frac{\delta g^{\text{obs}} - C^v \delta u^{\text{obs}}}{C^{e,N} - C^v}, \qquad (9)$$

$$\delta g^v = -C^v \frac{\delta g^{\text{obs}} - C^{e,N} \delta u^{\text{obs}}}{C^{e,N} - C^v}. \qquad (10)$$

Therefore, the contributions δg^v and δu^v of the GIA and $\delta g^e + \delta g^N$ and δu^e of the PDIM change to the observed gravity rate and vertical velocity of the ground can be uniquely solved and directly estimated from gravity and geodetic observations and theoretical ratios (3) and (5).

So far, we have considered that the remote unloaded/loaded area is located beneath the horizontal plane passing through the observation point (JAMES and IVINS 1998; LE MEUR and HUYBRECHTS 2001; MÄKINEN *et al.* 2007). However, since the Newtonian part of the gravity depends on the relative position of the observation point and location where mass changes occur (MERRIAM 1992; BOY *et al.* 2002; MÉMIN *et al.* 2009), it depends on the topography of the loaded area. In the next section, we examine the influences of the geophysical context, topography and load variation on $C^{e,N}$.

3. Study of $C^{e,N}$

3.1. $C^{e,N}$ in Areas Subject to both Past and Present-Day Ice-Mass Changes

The expressions (7)–(10) are valid if $C^{e,N}$ is known, which seems to be the case when the topography is neglected (Sect. 2.2), and if $C^{e,N} \neq C^v$. It is, indeed, impossible to discriminate processes producing the same gravity variation-to-vertical displacement ratio.

To put constraints on $C^{e,N}$, we consider the ratio $\delta u^v/\delta u^e$. Let us first assume that δu^e and δu^v have the same sign, so $\delta u^v/\delta u^e$ is positive. Therefore,

$$\frac{\delta u^v}{\delta u^e} = -\frac{\delta g^{\text{obs}} - C^{e,N} \delta u^{\text{obs}}}{\delta g^{\text{obs}} - C^v \delta u^{\text{obs}}} \geq 0, \qquad (11)$$

and

$$C^{e,N} \begin{cases} \geq \frac{\delta g^{\text{obs}}}{\delta u^{\text{obs}}}, & \text{if } \delta g^{\text{obs}} - C^v \delta u^{\text{obs}} > 0 \\ \leq \frac{\delta g^{\text{obs}}}{\delta u^{\text{obs}}}, & \text{if } \delta g^{\text{obs}} - C^v \delta u^{\text{obs}} < 0 \end{cases}. \qquad (12)$$

If, moreover, $\frac{\delta u^v}{\delta u^e} < 1$, then $C^{e,N}$ satisfies the following conditions:

$$C^{e,N} \begin{cases} \leq 2\dfrac{\delta g^{\mathrm{obs}}}{\delta u^{\mathrm{obs}}} - C^v, & \text{if } \delta g^{\mathrm{obs}} - C^v \delta u^{\mathrm{obs}} > 0 \\ \geq 2\dfrac{\delta g^{\mathrm{obs}}}{\delta u^{\mathrm{obs}}} - C^v, & \text{if } \delta g^{\mathrm{obs}} - C^v \delta u^{\mathrm{obs}} < 0 \end{cases}. \tag{13}$$

Second, we assume that δu^e and δu^v have opposite signs. Therefore,

$$C^{e,N} \begin{cases} \leq \dfrac{\delta g^{\mathrm{obs}}}{\delta u^{\mathrm{obs}}}, & \text{if } \delta g^{\mathrm{obs}} - C^v \delta u^{\mathrm{obs}} > 0 \\ \geq \dfrac{\delta g^{\mathrm{obs}}}{\delta u^{\mathrm{obs}}}, & \text{if } \delta g^{\mathrm{obs}} - C^v \delta u^{\mathrm{obs}} < 0 \end{cases}. \tag{14}$$

If, moreover, $\delta u^v / \delta u^e > -1$, then

$$C^{e,N} \begin{cases} > C^v, & \text{if } \delta g^{\mathrm{obs}} - C^v \delta u^{\mathrm{obs}} > 0 \\ < C^v, & \text{if } \delta g^{\mathrm{obs}} - C^v \delta u^{\mathrm{obs}} < 0 \end{cases}. \tag{15}$$

If $\delta u^v / \delta u^e = -1$, then $C^{e,N} = C^v$ and expressions (7) and (8) are no longer valid. The case $|\delta u^v / \delta u^e| > 1$ concerns either local ice-mass change which induces effects lower than that induced by the Pleistocene deglaciation or ice-mass change which is too remote to have sufficiently large effects. The different inequalities are shown in Fig. 1.

In conclusion, knowing the observed gravity and vertical displacement rates, as well as the glaciation and deglaciation context, we can provide a range of values for $C^{e,N}$.

In Sects. 3.2 and 3.3, we take now the topography into account for calculating $C^{e,N}$.

3.2. Expression for $C^{e,N}$

According to Eq. 5,

$$C^{e,N} = \frac{\delta g^e + \delta g^N}{\delta u^e}. \tag{16}$$

In this section we derive an expression for $C^{e,N}$ that explicitly contains the distance between the observation site and the location where the loading is applied. The derived expression is used in Sect. 3.3 to study the influence of the topography on $C^{e,N}$.

In spherical coordinates r, θ, ϕ, the Newtonian (δg^N) and elastic (δg^e) gravity variations and the vertical displacement rate (δu^e) are respectively given by

$$\delta g^N(\mathbf{r}) = \iiint_v \rho(\mathbf{r}') G_{g^n}(\mathbf{r}, \mathbf{r}') r'^2 \mathrm{d}r' \sin\theta' \mathrm{d}\theta' \mathrm{d}\phi' \tag{17}$$
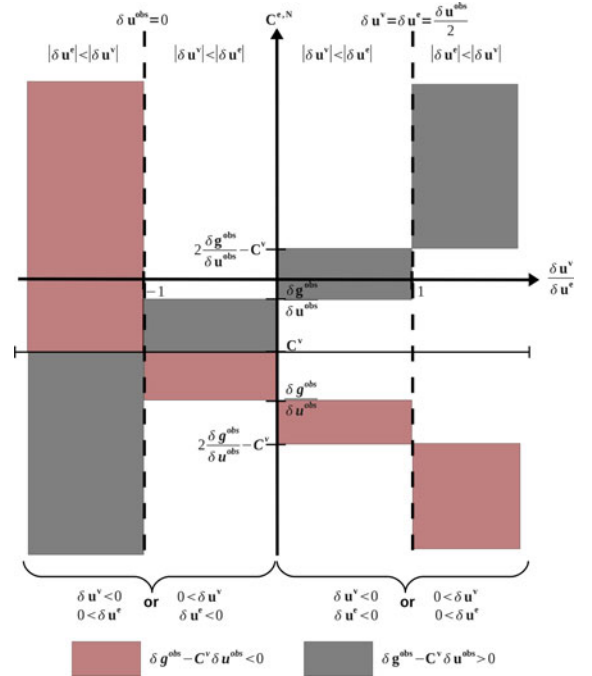

Figure 1
Summary of the different cases, corresponding to various geophysical processes, discussed in the text for the ratio $C^{e,N}$

$$\delta g^e(\mathbf{r}) = \iint_\Omega \rho(\mathbf{r}') \delta h(\mathbf{r}') G_{g^e}(\mathbf{r} - \mathbf{r}') r'^2 \sin\theta' \mathrm{d}\theta' \mathrm{d}\phi' \tag{18}$$

$$\delta u^e(\mathbf{r}) = \iint_\Omega \rho(\mathbf{r}') \delta h(\mathbf{r}') G_{u^e}(\mathbf{r} - \mathbf{r}') r'^2 \sin\theta' \mathrm{d}\theta' \mathrm{d}\phi', \tag{19}$$

where $\mathbf{r}'$ is the position of an element of ice-height variation δh and density ρ. The surface and volume of the ice load are, respectively, Ω and v. Green functions for the vertical displacement and elastic gravity variations are respectively (Farrell 1972):

$$G_{u^e}(\mathbf{r} - \mathbf{r}') = \frac{G}{a g_0} \sum_{n=1}^{\infty} h_n' P_n(\cos\psi), \tag{20}$$

$$G_{g^e}(\mathbf{r} - \mathbf{r}') = -\frac{G}{a^2} \sum_{n=1}^{\infty} \left[2h_n' - (n+1)k_n' \right] P_n(\cos\psi). \tag{21}$$

G is the Newtonian constant of gravitation and g_0, the gravity at the surface of the spherical Earth model of

mean radius a. h'_n and k'_n are the load Love numbers of degree n for the displacement and variation of the gravity potential respectively. P_n is the Legendre polynomial of degree n. ψ is the angular distance between the observation point and loading point. The Green function for the Newtonian gravity variation is (MERRIAM 1992; BOY et al. 2002):

$$G_{g^n}(\mathbf{r}, \mathbf{r}') = G \frac{r - r' \cos \psi}{(r^2 + r'^2 - 2rr' \cos \psi)^{3/2}}. \qquad (22)$$

Angular distance ψ is given by

$$\cos \psi = \cos \theta \cos \theta' + \sin \theta \sin \theta' \cos(\phi - \phi'). \quad (23)$$

Inserting Eqs. 17–22 in Eq. 16 and assuming a constant density for the load, we obtain

$$C^{e,N}(\mathbf{r}) = \frac{\rho}{\delta u^e(\mathbf{r})} \iint\limits_{\Omega}$$
$$\left[\delta h(\mathbf{r}') G_{g^e}(\mathbf{r} - \mathbf{r}') r'^2 + \int\limits_{r'}^{r'+\delta h(\mathbf{r}')} G_{g^n}(\mathbf{r}, \mathbf{r}'_1) r_1'^2 dr'_1 \right]$$
$$\sin \theta' \mathrm{d}\theta' \mathrm{d}\phi',$$
$$(24)$$

where the coordinates of the point at $\mathbf{r}'_1$ are $r' + \mathrm{d}z', \theta', \phi'$. One can rewrite Eq. 24

$$C^{e,N}(\mathbf{r}) = \frac{\rho}{\delta u^e(\mathbf{r})} \iint\limits_{\Omega} \left[\delta h(\mathbf{r}') G_{g^e}(\mathbf{r} - \mathbf{r}') r'^2 \right.$$
$$\left. + \int\limits_{0}^{\delta h(\mathbf{r}')} G_{g^n}(\mathbf{r}, \mathbf{r}' + z' \mathbf{e_r})(r' + z')^2 \mathrm{d}z' \right]$$
$$\sin \theta' \mathrm{d}\theta' \mathrm{d}\phi'. \qquad (25)$$

If we denote by z^{load} and z^{obs} respectively the altitudes of the loading point and observation point, then $r' = a + z^{\mathrm{load}} \gg z'$ and $r = a + z^{\mathrm{obs}}$. Thus, we obtain

$$C^{e,N}(\mathbf{r}) = \frac{\rho}{\delta u^e(\mathbf{r})} \iint\limits_{\Omega} \left[\delta h(\mathbf{r}') G_{g^e}(\mathbf{r} - \mathbf{r}') r'^2 \right.$$
$$\left. + \int\limits_{0}^{\delta h(\mathbf{r}')} G_{g^n}(\theta - \theta', \phi - \phi', z^{\mathrm{obs}} - z^{\mathrm{load}} - z') r'^2 \mathrm{d}z' \right]$$
$$\times \sin \theta' \mathrm{d}\theta' \mathrm{d}\phi' \qquad (26)$$

or

$$C^{e,N}(\mathbf{r}) = \frac{\rho}{\delta u^e(\mathbf{r})} \iint\limits_{\Omega} \left[\delta h(\mathbf{r}') G_{g^e}(\mathbf{r} - \mathbf{r}') \right.$$
$$\left. + \int\limits_{z^{\mathrm{load}}}^{z^{\mathrm{load}}+\delta h(\mathbf{r}')} G_{g^n}(\theta - \theta', \phi - \phi', z^{\mathrm{obs}} - z') \mathrm{d}z' \right]$$
$$\times r'^2 \sin \theta' \mathrm{d}\theta' \mathrm{d}\phi'. \qquad (27)$$

We introduce the pseudo Green function of $C^{e,N}$ that we name $G_{C^{e,N}}(\mathbf{r}, \mathbf{r}')$. Actually, $G_{C^{e,N}}$ is a function of $\mathbf{r} - \mathbf{r}'$:

$$G_{C^{e,N}}(\mathbf{r} - \mathbf{r}') = \frac{1}{\delta h(\mathbf{r}') G_{u^e}(\mathbf{r} - \mathbf{r}')} \left[\delta h(\mathbf{r}') G_{g^e}(\mathbf{r} - \mathbf{r}') \right.$$
$$\left. + \int\limits_{z^{\mathrm{load}}}^{z^{\mathrm{load}}+\delta h(\mathbf{r}')} G_{g^n}(\theta - \theta', \phi - \phi', z^{\mathrm{obs}} - z') \mathrm{d}z' \right]$$
$$(28)$$

We call it a pseudo Green function because it is the ratio produced by a mass point of height δh, in other terms, it is a unit-mass point response scaled to δh. Using Eq. 28, Eq. 16 transforms to

$$C^{e,N}(\mathbf{r}) = \frac{\rho}{\delta u^e(\mathbf{r})} \iint\limits_{\Omega} \delta h(\mathbf{r}') G_{u^e}(\mathbf{r} - \mathbf{r}') G_{C^{e,N}}(\mathbf{r} - \mathbf{r}')$$
$$\times r'^2 \sin \theta' \mathrm{d}\theta' \mathrm{d}\phi'. \qquad (29)$$

We now write

$$\alpha(\mathbf{r}, \mathbf{r}') = \delta h(\mathbf{r}') \frac{G_{u^e}(\mathbf{r} - \mathbf{r}')}{\delta u^e(\mathbf{r})}, \qquad (30)$$

and introduce it in Eq. 29. We finally obtain

$$C^{e,N}(\mathbf{r}) = \rho \iint\limits_{\Omega} \alpha(\mathbf{r}, \mathbf{r}') G_{C^{e,N}}(\mathbf{r} - \mathbf{r}') r'^2 \sin \theta' \mathrm{d}\theta' \mathrm{d}\phi'.$$
$$(31)$$

Thus, as predicted, $C^{e,N}$ depends on the distance between the observation and loading points and, consequently, on the surface of the load. It also depends on the ice-height variations at each loading point. Function α is a weighting factor that indicates how $C^{e,N}$ for a specific loading point contributes to the total $C^{e,N}$ ratio induced by the whole load. Its

behaviour is shown in Fig. 2, where $\alpha\delta u^e/\delta h$ is plotted. For example, loading points located either 200 km or 1 km from the observation point have the same weight if the height variation of the farthest loading point is almost 1,000 times larger than that of the closest. Consequently, the contribution of the $C^{e,N}$ ratio of one specific loading point is strongly influenced by the ice-height variation if it is larger than that of other further away loading points.

3.3. Study of $G_{C^{e,N}}$

Using the Green functions for the deformation of a symmetric, non-rotating, elastically isotropic Earth model (FARRELL 1972), we compute $G_{C^{e,N}}$ for $\delta h = 1$ m/year of water ($\rho = 1,000$ kg m^{-3}). The observation points are at a distance ranging from 1 to 1,111 km from the loading point. To take into account the influence of the topography, namely the relative elevation between the load and the observation point, we compute $G_{C^{e,N}}$ for a load located at several altitudes ($z^{\text{load}} \in [0; 2,000]$ m). The altitude of the observation point is $z^{\text{obs}} = 1,000$ m. The difference between the altitudes of the observation point and load is $\Delta z = z^{\text{load}} - z^{\text{obs}}$. Plots are shown in Fig. 3.

First, we show that $G_{C^{e,N}} \sim -0.26$ μGal/mm for $\Delta z = 0$ m. This is valid for a point load acting at any distance from the observation site. Consequently, for any load, we have $C^{e,N} \sim -0.26$ μGal/mm, as found by de LINAGE et al. (2007).

Next, $G_{C^{e,N}}$ varies very differently closer to the observation point according to Δz. The strong increase toward positive numbers for $\Delta z \geq 0$ is because mass changes are above the observation point. Increasing (resp. decreasing) the mass decreases (resp. increases) the gravity and leads to a negative (resp. positive) gravity variation. Because of an increased (resp. a decreased) mass, the ground subsides (resp. uplifts) and a negative (resp. positive) displacement variation can be observed. Consequently, the resulting ratio is positive. If $\Delta z \leq 0$, the mass changes beneath the observation site and $G_{C^{e,N}}$ strongly decreases for both increasing and decreasing masses. Indeed, the gravity variation and vertical velocity have opposite signs in these cases. Otherwise, with the distance the ratios converge to that obtained for $\Delta z = 0$, namely about -0.26 μGal/mm.

We repeat the same computation for $\delta h = \{2, 5, 10, 50, 100\}$ m/year and denoting $G_{C^{e,N}}^1(\mathbf{r} - \mathbf{r}')$ the function $G_{C^{e,N}}(\mathbf{r} - \mathbf{r}')$ for $\delta h = 1$ m/year, we plot

$$\Delta G_{C^{e,N}}(\mathbf{r} - \mathbf{r}') = \text{Log}|G_{C^{e,N}}^1(\mathbf{r} - \mathbf{r}') - G_{C^{e,N}}(\mathbf{r} - \mathbf{r}')| \tag{32}$$

on Figs. 4 and 5 for several relative altitudes. We study the influence of the load variation rate δh. We obtain:

- $\Delta G_{C^{e,N}}$ increases with the distance to the load for any Δz, it is about 0.01 μGal/mm at 50 km from the loading point for $|\delta h| = 100$ m/year,
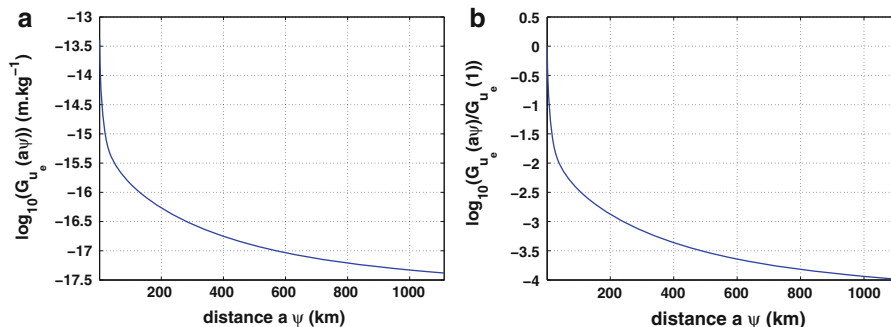

Figure 2
Weighting factor $\alpha\delta u^e/\delta h$ plotted as a function of the distance of the observation point from the load (*left*) and divided by that computed for an observation point located at 1 km from the load (*right*)
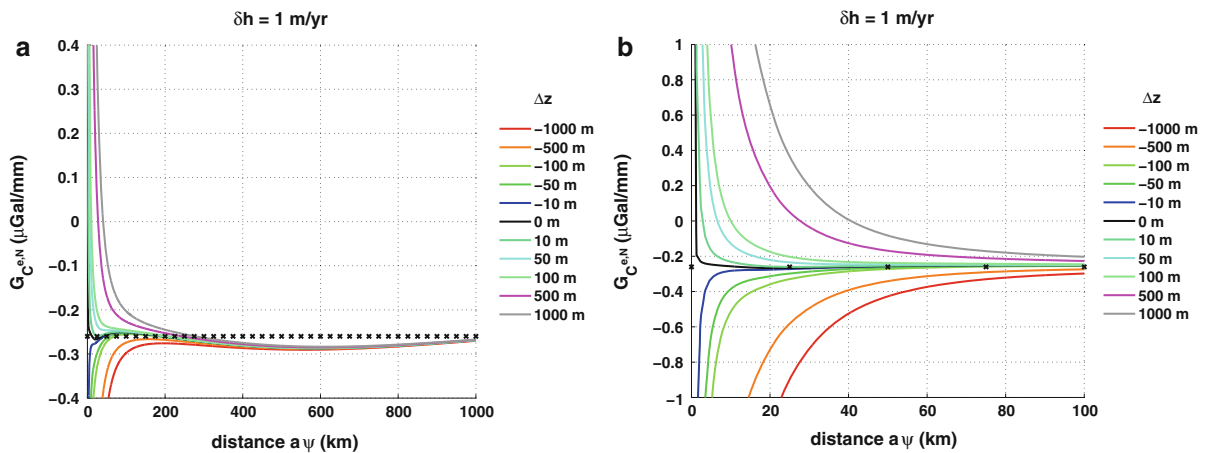
Figure 3

$G_{C^{e,N}}$ as a function of the distance to the observation point from the load for $\delta h = 1$ m/year and several relative altitudes $\Delta z = z^{\text{load}} - z^{\text{obs}}$

- $\Delta G_{C^{e,N}} \leq 0.01\ \mu\text{Gal/mm}$ for $|\delta h| \leq 10$ m/year from 11 km from the loading point,
- $\Delta G_{C^{e,N}} \leq 0.01\ \mu\text{Gal/mm}$ for $|\delta h| \leq 5$ m/year from 6.5 km from the loading point,
- $\Delta G_{C^{e,N}} \leq 0.08\ \mu\text{Gal/mm}$ for $|\delta h| \leq 5$ m/year from 2 km from the loading point.

If we have a digital elevation model and if load variations are farther than 2 km away from the observation point, we can estimate $G_{C^{e,N}}$ independently of the load variations and Δz if height variations are lower than 5 m/year. In that case, the accuracy is better than 0.08 μGal/mm. The accuracy would be better than 0.02 μGal/mm if $|\delta h| \leq 2$ m/year. For distances farther than 6.5 or 11 km, the load variation has to be lower than 5 or 10 m/year respectively to have $G_{C^{e,N}}$ with 0.01 μGal/mm accuracy.

However, the topography of the load is not sufficient to completely determine the total $C^{e,N}$ ratio induced by a load acting on any area that would allow the unique determination of the contributions from the GIA and the PDIM change. Indeed, the height variations of the load appear in the coefficient α (Eq. 30) and need to be known. So, in Sect. 4, we review the specific case of Svalbard, which has already been studied (SATO *et al.* 2006; MÉMIN *et al.* 2011), and focus on what can be extracted from the $C^{e,N}$ ratio.

4. Past and Present-Day Ice-Mass Changes in Svalbard

4.1. Location of Svalbard and Geodetic Observations

4.1.1 Svalbard Archipelago and Ny-Ålesund Observatory

The Arctic archipelago of Svalbard is located north of Norway between 76°N and 81°N of latitude and 11°E and 26°E of longitude. It is covered by about 36,000 km^2 of ice which represents 60 % of the total area. Most of the ice surface is thinning (KOHLER *et al.* 2007; DOWDESWELL *et al.* 2008; KÄÄB 2008; MOHOLDT *et al.* 2009; NUTH *et al.* 2010), which induces deformation and gravity variations. Svalbard is also subject to the GIA following the last deglaciation (e.g. TUSHINGHAM and PELTIER 1991). At the Geodetic Observatory of Ny-Ålesund (11.855°E, 78.929°N, 43 m), Very Long Baseline Interferometry (VLBI), GPS or Doppler Orbitography and Radiopositioning Integrated by Satellite (DORIS) data have been collected for up to 18 years. The gravity variation is measured since 1999 with a superconducting gravimeter, which is part of the Global Geodynamics Project (CROSSLEY *et al.* 1999), and the absolute gravity has been measured six times with FG5 absolute gravimeters: in 1998, 2000, 2001, 2002, 2004, and 2007.
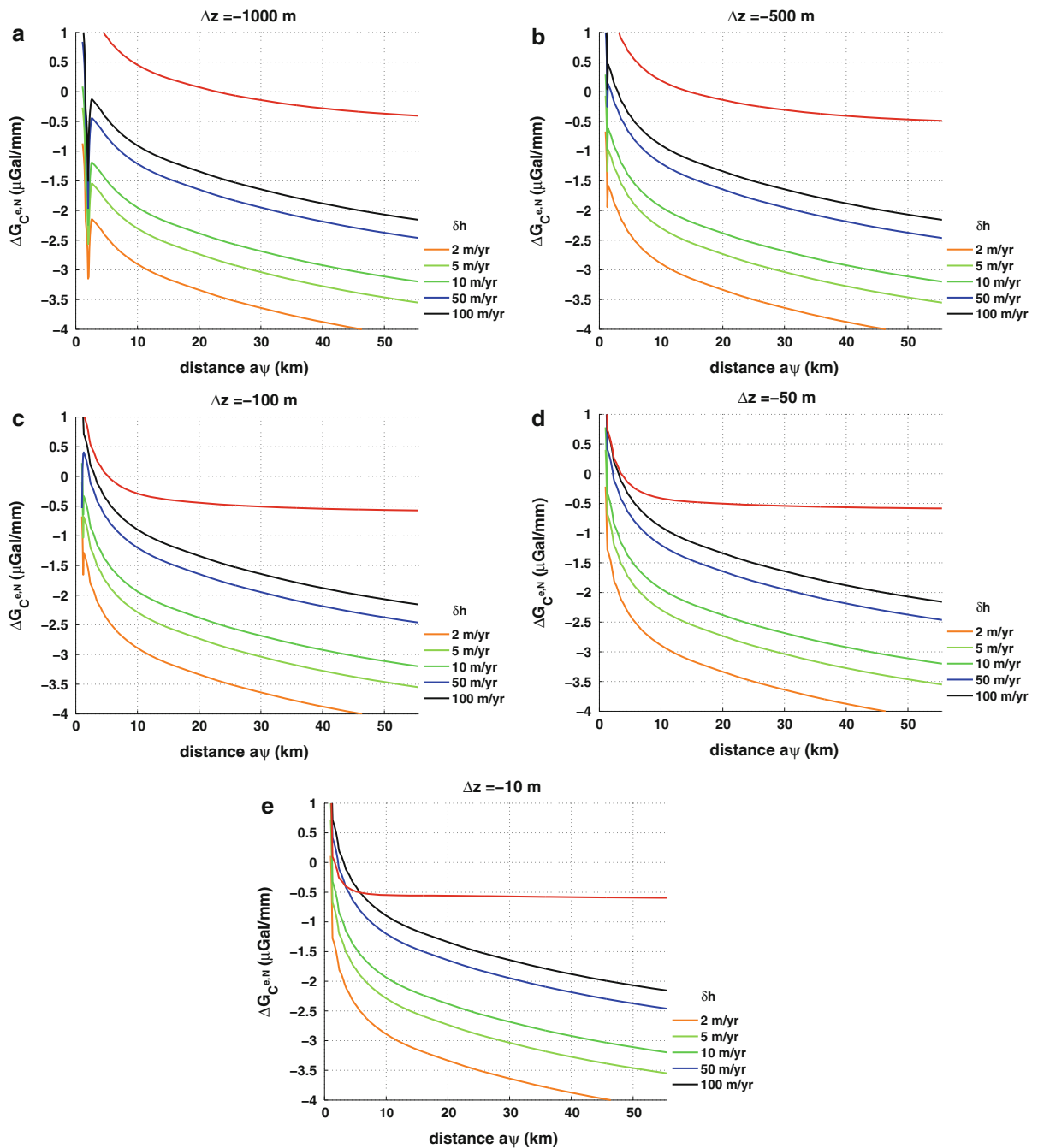
Figure 4

$G_{C^{e,N}}(\mathbf{r} - \mathbf{r'})$ computed for $\delta h = 1$ m/year (*red curve*) and $\Delta G_{C^{e,N}}$ (*other color curves*) as a function of the distance of the observation point from the load for five relative altitudes ($\Delta z = z^{load} - z^{obs} < 0$). $\Delta G_{C^{e,N}}$ is computed for five load variations ($\delta h = \{2, 5, 10, 50, 100\}$ m/year)

The Digital Chart of the World (DCW, http://www.maproom.psu.edu/dcw/) provides a realistic geographical distribution of the glaciers. More accurate location and altitude of the glaciers near Ny-Ålesund are given by the Digital Elevation Model (DEM) from the SPIRIT project (KORONA *et al.*
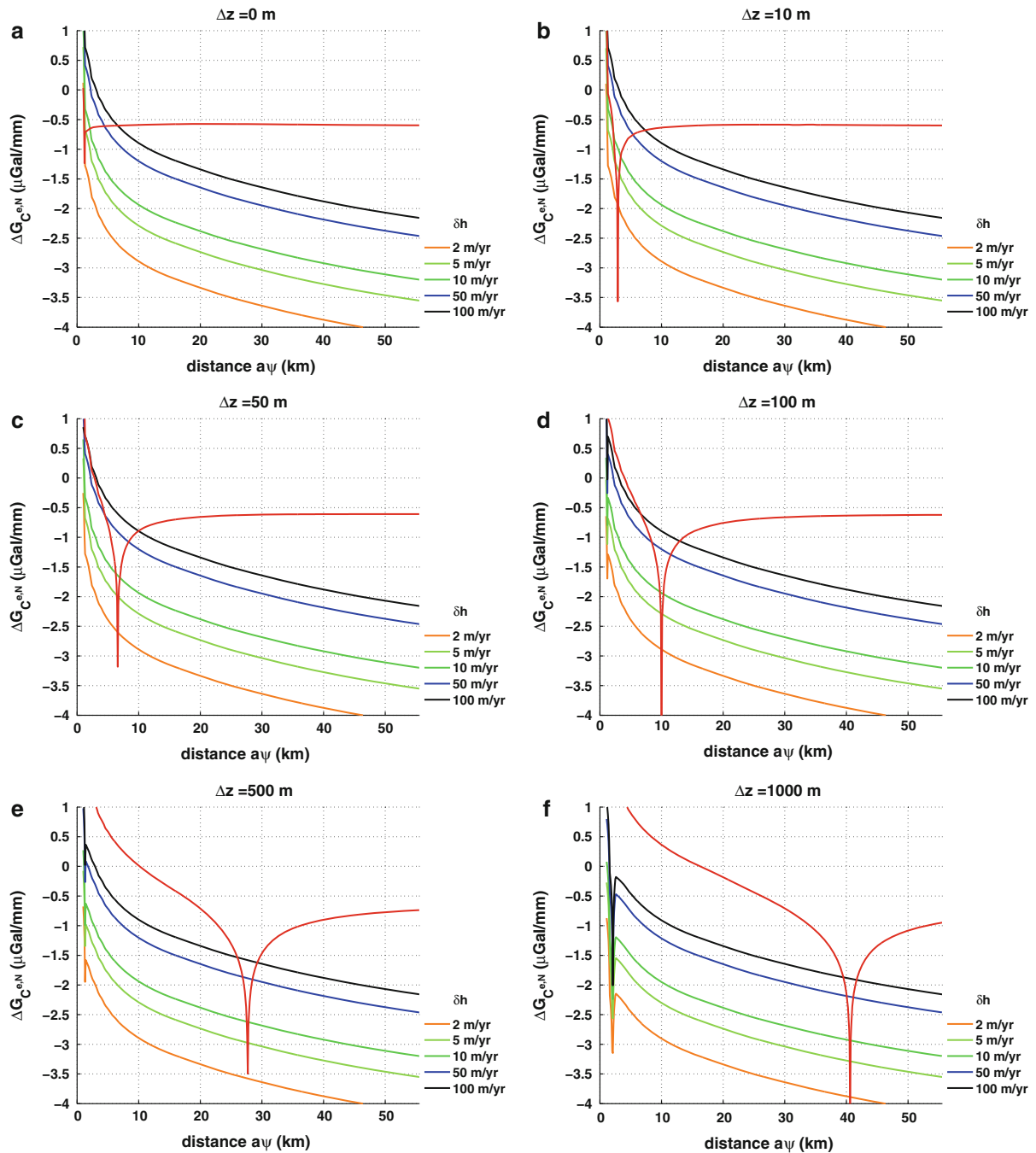
Figure 5
Same as Fig. 4 for six other relative altitudes ($\Delta z = z^{\text{load}} - z^{\text{obs}} \geq 0$)

2009). For all the other glaciers, the topography is provided by the GTOPO30 DEM (http://edc.usgs.gov/products/elevation/gtopo30/gtopo30.html). The total surface of ice is divided into seven basins as shown in Fig. 6.

4.1.2 Observations at Ny-Ålesund

Sato *et al.* (2006) obtained from VLBI, GPS and gravity observations an uplift rate of 5.2 ± 0.6 mm/year and a gravity rate of -2.5 ± 0.9 μGal/year at

Ny-Ålesund. These rates have been revised by MÉMIN et al. (2011) using longer datasets. They use six absolute gravity measurements for the period 1998–2007, instead of four for SATO et al. (2006) for the period 1998–2002, and find a lower value of -1.02 ± 0.48 μGal/year. They propose an uplift rate of 5.64 ± 1.57 mm/year using velocity observations found in the literature. A direct modeling of their observations with a uniform ice-mass loss rate of 75 cm/year allows to fit the observations. This rate is consistent with the one proposed by SATO et al. (2006). However, the corresponding volume of ice loss, ~ 25 km^3/year, is larger than the one derived from the analysis of the GRACE data (MÉMIN et al. 2011) which is ranging between 5 and 18 km^3/year. The GRACE derived volume of ice loss is in agreement with glaciological studies estimating ice loss to be between 4 and 14.2 km^3/year. They associate a part of the discrepancy between ice losses derived from ground and space observations to be due to the difference of sensitivity of both methods.

Indeed GRACE measurements are mostly sensitive to the total loss of mass while ground gravity measurements are sensitive to local effects. To reduce the discrepancy, they propose to take into account the altitude dependency of ice-mass change in the modeling of PDIM change effects. Using ground observations, we evaluate non uniform ice-mass change scenarios by focusing on the $C^{e,N}$ ratio.

4.2. Ice-Mass Change Distribution in Svalbard

4.2.1 Glaciers Distribution in Svalbard with Respect to Ny-Ålesund Observatory

Figure 7 shows the distribution of area of basin 1, as a function of altitude and distance to Ny-Ålesund observatory, relative to the total area of the seven basins. All the glaciers in this basin, which is the smallest, are located above Ny-Ålesund. Moreover, a large part ($\sim 25\%$) of the ice in this region is located between 2 and 5 km from the station and between 40
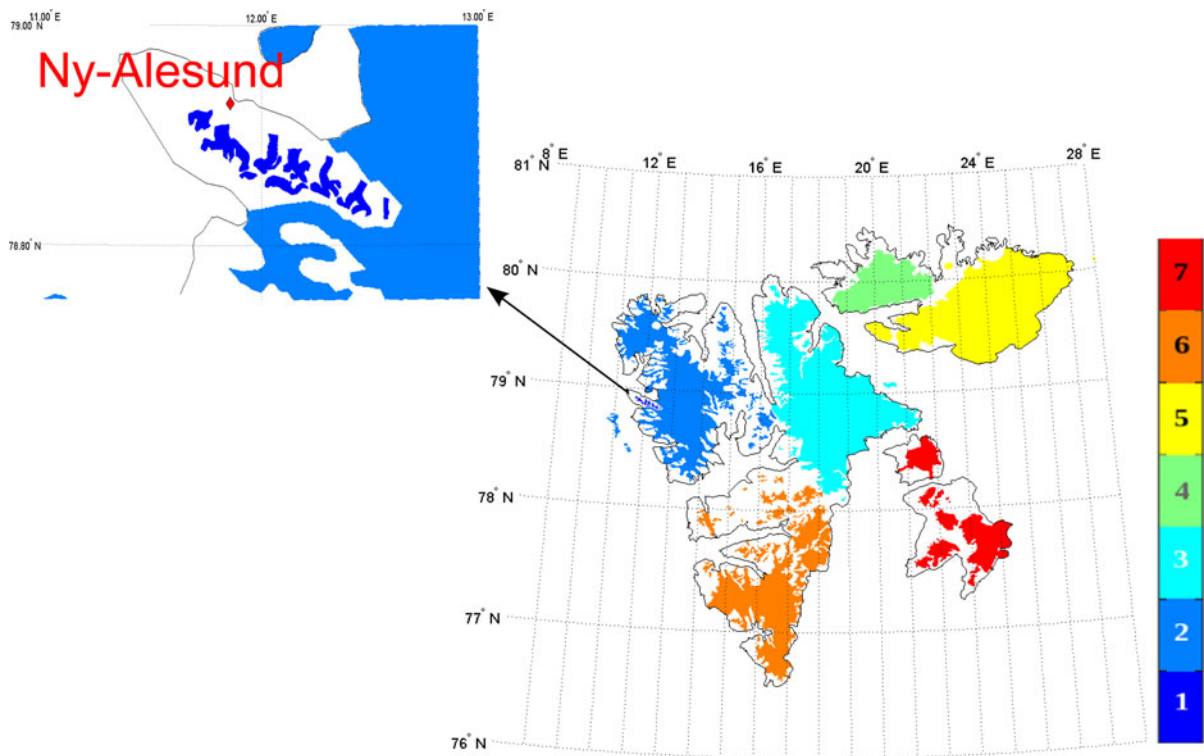

Figure 6
Ice-covered area in Svalbard from the Digital Chard of the World. The total surface is divided into seven basins, whose numbers appear in the *color bar* on the *right* of the map
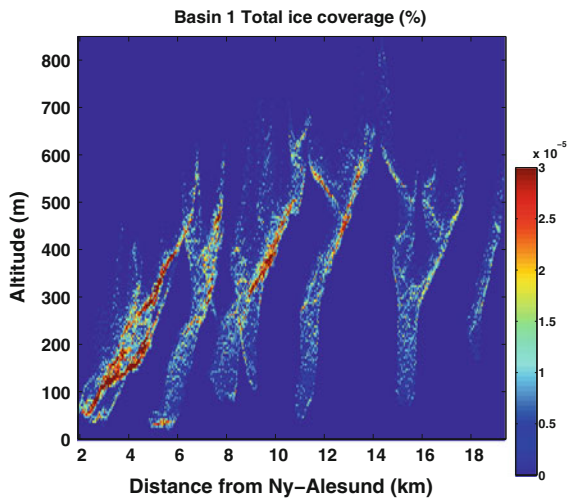
Figure 7
Distribution of ice-covered area (%) for basin 1, scaled to the total area of ice coverage, as a function of both the distance from Ny-Ålesund and altitude of the load

and 500 m of altitude. Figure 8 shows the distribution of the ice in each basin as a function of the distance to the station. Basin 2 extends from 10 to 110 km, basin 3 from 100 to 210 km, basin 4 from 165 to 240 km, basin 5 from 175 to 350 km, basin 6 from 115 to 280 km, and basin 7 from 205 to 320 km.

4.2.2 Ice-Mass Change Profiles

Figure 9 shows the rate of the thickness variation, dh/dt, of the ice load for the seven basins as a function of the altitude. We assume that, for a given altitude, dh/dt is the same over an entire basin. The profiles for basins 3, 4, 6 and 7 are based on the study by NUTH

et al. (2010). The profile for basin 5 is based on the study by MOHOLDT *et al.* (2009). For both basins 1 and 2, we consider two different profiles, labelled 1a, 1b, 2a and 2b. Profiles 1a and 1b are obtained from the height change rates provided by KOHLER *et al.* (2007). Profile 2a is also given by NUTH *et al.* (2010). Finally, we derive profile 2b by using an average of the thinning rates provided by KIERULF *et al.* (2009).

4.3. Gravity and Uplift Rates at Ny-Ålesund

4.3.1 Computation of Gravity and Uplift Rates

The geodetic effects of ice-mass change are numerically calculated with account for the geographic distribution and topographic height of the glaciers. The total gravity rates or vertical velocity at the observation station are obtained using Eqs. 17–19 of Sect. 2 assuming that the load has a uniform density $\rho = 1{,}000$ kg/m^3.

The computed vertical motion and gravity rate at Ny-Ålesund for five models of ice-mass change are listed in Table 1. In models 1, 2, and 5, we use profiles 3–7. In models 1 and 2, we respectively use the couple of profiles 1a–2a and 1b–2b. In models 3 and 4, we assume a uniform thinning rate of 1 m/year. In model 4, we do not take into account the topography of the glaciers. Model 5 is the same as model 2 but the profile 2b is multiplied by 2. This increases the thinning or thickening rates and changes the ice loss. These five models will allow us to study the influence of (1) the topography of the glaciers on the geodetic consequences of ice-mass change and (2)
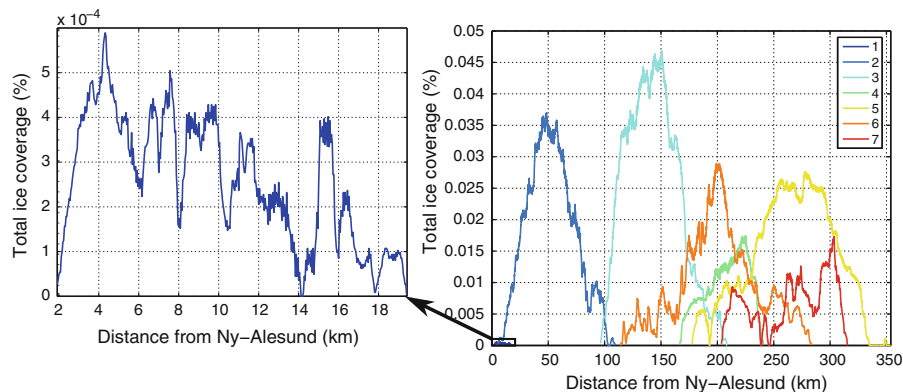

Figure 8
Distribution of ice-covered area (%) for each basin of Fig. 6 as a function of the distance from Ny-Ålesund
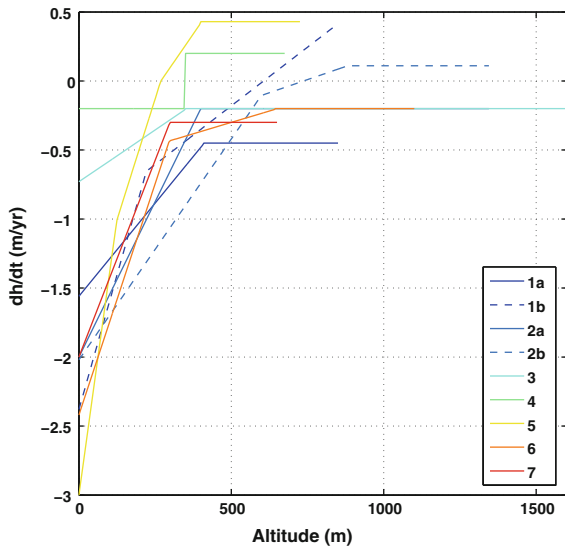
Figure 9

Rate of ice height change dh/dt as a function of the altitude for each basin of Fig. 6. *Curves 1a* and *1b* are used for basin 1 and *2a* and *2b* are used for basin 2

the geographical distribution of ice-mass change over a given glacier.

4.3.2 Study of Different Ice-Mass Change Scenarios

Comparison of models 3 and 4 in Table 1 shows that the topography plays a role only for the closest glaciers, in basins 1 and 2. The influence on the

gravity rate of the mass variation of the glaciers in basins 3–7, which are more than 100 km away from the station, is so small that their topography does not need to be taken into account.

Figure 10 shows the computed gravity rates as a function of the uplift rates at Ny-Ålesund for the five models of ice-mass changes. It also shows the GIA effect (solid black line), corresponding to a slope of approximately -0.15 μGal/mm ratio (WAHR *et al.* 1995), and the elastic PDIM change effect without any topography (black dashed line), which corresponds to the -0.26 μGal/mm ratio theoretically found by de LINAGE *et al.* (2007). We assume that these two lines cross at the point which corresponds to the GIA effects computed by SATO *et al.* (2006) namely -1.88 mm/year for the vertical velocity and -0.31 μGal/year for the annual gravity rate.

We see in Fig. 10 that neither model 1 nor model 2 can explain observations within their error bars while models 3, 4 and 5 could. However, model 4 is discarded since no topography is taken into account. If we consider a model similar to model 3, but with a uniform ice-mass change rate of -0.85 m/year, we obtain 3.60 mm/year for the vertical velocity and -0.37 μGal/year for the annual gravity rate. These values are very close to the ones found for model 5 (3.52 mm/year and -0.39 μGal/year), see Fig. 10. But, the annual ice losses are very different for the

Table 1

At Ny-Ålesund, vertical velocity δu^e (mm/year) and total gravity rate $\delta g^{e+N} = \delta g^e + \delta g^N$ (μGal/year) due to ice-mass change

Model		1		2			3	4	5	
dh/dt profiles		1a, 2a, 3–7		1b, 2b, 3–7			-1 m/year		1b, $2 \times$ 2b, 3–7	
Volume of ice loss (km³/year)		-11.64		-12.22			-35.48		-15.67	
Basin	Area (km²)	δu^e	δg^{e+N}	δu^e	δg^{e+N}	δu^e	δg^{e+N}	δg^{e+N*}	δu^e	δg^{e+N}
1	40	0.175	0.198	0.166	0.172	0.191	0.226	-0.046	0.166	0.172
2	6,411	1.21	-0.175	1.43	-0.219	2.37	-0.231	-0.626	2.86	-0.439
3	9,453	0.208	-0.050	0.208	-0.050	0.844	-0.201	-0.216	0.208	-0.050
4	2,543	-0.0622	0.0016	-0.0622	0.0016	0.127	-0.033	-0.0339	-0.0622	0.0016
5	8,419	0.0232	-0.00667	0.0232	-0.00667	0.289	-0.0785	-0.0795	0.0232	-0.00667
6	5,875	0.211	-0.055	0.211	-0.055	0.320	-0.0827	-0.0847	0.211	-0.055
7	2,741	0.0576	-0.0158	0.0576	-0.0158	0.0928	-0.0253	-0.0256	0.0576	-0.0158
Total	35,482	1.88	-0.10	2.09	-0.17	4.23	-0.43	-1.11	3.52	-0.39
Total with GIA		3.76	-0.41	3.97	-0.48	6.11	-0.74	-1.42	5.4	-0.7
$\delta g^{e+N}/\delta u^e$ (μGal/mm)		-0.06		-0.08			-0.10	-0.26	-0.11	

δg^{e+N*} is the gravity variation computed without taking into account the topography of the changing glaciers. According to SATO *et al.* (2006), the uplift and gravity variation associated to the GIA are, respectively, 1.88 mm/year and -0.31 μGal/year

two models: it is approximately 30 km³/year for the former and 15 km³/year for the latter. Even if the model 3 scaled to −0.85 m/year could explain ground observations, it does not explain GRACE satellite gravimetric measurements. Model 5 is more appropriate to explain both the ground and space observations.

4.4. $C^{e,N}$ at Ny-Ålesund, Svalbard

4.4.1 Results of Modelling

The influence of the topography in basins 1 and 2 is significant: if we take it into account, the gravity rate to vertical velocity ratio is −0.10 μGal/mm, while we obtained −0.26 μGal/mm in Sect. 2, where the topography was neglected. We have checked that other uniform thinning rates lead to the same $C^{e,N}$
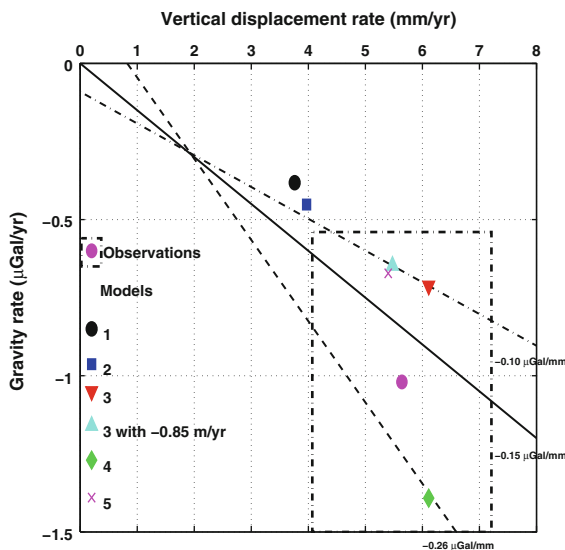
Figure 10

Computed gravity rate as a function of the uplift rate at Ny-Ålesund. The *solid black line* gives the GIA effect. Its slope is approximately −0.15 μGal/mm (WAHR *et al.* 1995). The *black dashed line* corresponds to the −0.26 μGal/mm ratio theoretically found by de LINAGE *et al.* (2007) for the elastic PDIM change effect without any topography. The *black dotted dashed line* corresponds to the −0.10 μGal/mm ratio found for different values of ice-thinning rate with the model 3. All *these lines* cross at the point which corresponds to the GIA effects computed by SATO *et al.* (2006). The *black symbols* are the computed rates for the model 1 (*circle*), 2 (*square*), 3 (*inverted triangle*), 4 (*diamond*) and 5 (*cross*). The *triangle* corresponds to the model 3 with a uniform ice thinning of 0.85 m/year. Observations (*magenta circle*) are from MÉMIN *et al.* (2011)

(black dotted dashed line on Fig. 10). This is a direct consequence of the results of Sect. 3 for $|\delta h| \leq 1$ m/year. Therefore, if one considers a uniform loading, the problem of Sect. 2 is still uniquely solved even if the topography is taken into account.

Comparison of models 1, 2 and 5 shows that $\delta g^e + \delta g^N$ and δu^e at Ny-Ålesund, as well as $C^{e,N}$, depend on the spatial distribution of ice-mass change over basins 1 and 2. For models 1, 2, 3 and 5, the absolute value of $C^{e,N}$ is 2–4 times smaller than for model 4, in which the topography is neglected.

Figure 11 shows $C^{e,N}$ due to ice-mass change in each basin separately. For basins 1 and 2, the ratio is clearly dependent on the load while for basins 3 to 7, the ratio is close to −0.26 μGal/mm in agreement with results of Sect. 3. When the topography is not taken into account, the ratio is close to −0.26 μGal/mm for all the basins as proposed by de LINAGE *et al.* (2007).

4.4.2 $C^{e,N}$ Estimated from Observations

The gravity and vertical displacement variations at Ny-Ålesund are, respectively, −1.02 μGal/year and 5.64 mm/year (Sect. 1) leading to $\delta g^{\text{obs}}/\delta u^{\text{obs}} = -0.18$ μGal/mm and $\delta g^{\text{obs}} - C^v \, \delta u^{\text{obs}} < 0$.

Knowing that most of ice in Svalbard is thinning and that Ny-Ålesund is subject to the uplift due to the Pleistocene deglaciation, then according to Sect. 1, $C^{e,N}$ should be lower than −0.18 μGal/mm. Besides, if displacement variations due to PDIM are larger than those due to GIA, then $C^{e,N}$ should be higher than $2\delta g^{\text{obs}}/\delta u^{\text{obs}} - C^v = -0.21$ μGal/mm. When $C^{e,N}$ decreases from −0.18 μGal/mm, δu^v increases while δu^e decreases and for $C^{e,N} = -0.21$ μGal/mm, $\delta u^v = \delta u^e = \delta u^{\text{obs}}/2$.

The fact that $C^{e,N}$ can be different from −0.26 μGal/mm shows that ice-mass change occurs at different altitudes. Moreover, if $C^{e,N}$ is higher than −0.26 μGal/mm, this means that most of ice-mass surrounding Ny-Ålesund changes above the altitude of the observation site (Sect. 3). If $C^{e,N} = -0.26$ μGal/mm, GIA effects would be larger than PDIM change. The expected uplift rate induced by GIA would be, in this case, about 3.96 mm/year which is more than twice that modeled by SATO *et al.* (2006). Indeed, as seen in Sect. 3, they obtained
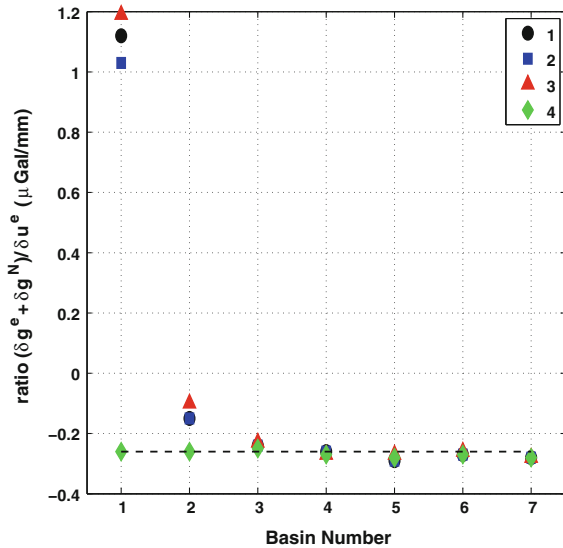
Figure 11
$C^{e,N}$ separately computed for each basin of Fig. 6, using the profiles of ice-mass change of Fig. 9 or a uniform thinning rate of 1 m/year. The *black dashed line* is -0.26 μGal/mm

$u^v = 1.88$ mm/year which leads to $u^e = 3.72$ mm/year and $C^{e,N} = -0.20$ μGal/mm. Using $C^{e,N} = -0.26$ μGal/mm leads to $u^e = 1.63$ mm/year.

From observations and the glaciation/deglaciation context we suggest that $C^{e,N}$ ranges between -0.21 and -0.18 μGal/mm whereas the best model provides -0.10 μGal/mm for the same context. The discrepancy is likely due to measurement accuracies which remain an important issue for the separation of geodetic consequences of GIA and PDIM change.

5. Conclusion

By modeling the elastic and viscoelastic deformations of the earth, one can compute the gravity variation-to-vertical displacement ratios C^v and $C^{e,N}$ that are defined for the GIA and PDIM change processes, respectively. They allow for a unique separation of the two effects, which are simultaneously observed by using geodetic and gravimetric techniques, provided one assumes the ice-mass change is uniform in a thin layer over the surface of the spherical model.

In this paper we have focused on $C^{e,N}$ and shown that according to the glaciation/deglaciation context

and from the measurement of gravity variation and ground vertical velocity one can deduce a range of possible values for the $C^{e,N}$ ratio. Introducing the pseudo Green function $G_{C^{e,N}}$ we have shown that $C^{e,N}$ not only depends on the topography but also on the height variation of the ice load. Studying $G_{C^{e,N}}$ for the influence of the topography, we have shown that $C^{e,N}$ tends to positive values if most of surrounding ice-mass changes above the altitude of the observation site and to values lower than -0.26 μGal/mm if it changes below. We have also shown that $G_{C^{e,N}}$ can be known independently from the ice-height variation using a DEM with a 0.01 μGal/mm accuracy provided the ice load is located at least 6.5 km from the observation site and its variations are lower than 5 m/year. However, in general, for short distances and large ice-height variations, the determination of $C^{e,N}$ from a DEM only is not possible.

Using a particular example in Svalbard we have pointed out that different changes of ice volume and different load distributions can give similar vertical displacements and gravity variations or similar gravity variation-to-vertical displacement-rate ratio at a single observation station. This is clearly important in regions involving glaciers where the thinning rate varies from one glacier to the other. We have shown that $C^{e,N}$ does not depend on the rate of ice-mass change if it is spatially uniform. In this case, $C^{e,N}$ is larger than when the topography is neglected, and -0.26 μGal/mm can be considered to be a lower limit for the effect of PDIM change. If the ice-mass change is not spatially uniform, $C^{e,N}$ depends on the rate of change of the closest ice-covered area.

REFERENCES

AMALVICT M., WILLIS P., WÖOPPELMANN G., IVINS E. R., BOUIN M.-N., TESTUT L., and HINDERER J., 2009. *Isostatic stability of the East Antarctic station Dumont d'Urville from long-term geodetic*

observations and geophysical models, Polar Research, doi: 10.1111/j.1751-8369.2008.00091.x.

BARLETTA V. R., SABADINI R., and BORDONI A., 2008. *Isolating the PGR signal in the GRACE data: impact on mass balance estimates in Antarctica and Greenland*, Geophys. J. Int., *172*, 18–30.

BERTHIER E., SCHIEFER E., CLARKE G. K. C., MENOUNOS B., and RÉMY F., 2010. *Contribution of Alaskan glaciers to sea-level rise derived from satellite imagery*, Nature Geoscience, *3*, 92–95, doi: 10.1038/NGEO737.

BEVIS M., KENDRICK E., SMALLEY R., DALZIEL I., CACCAMISE D., SASGEN I., HELSEN M., TAYLOR F. W., ZHOU H., BROWN A., RALEIGH D., WILLIS M., WILSON T., and KONFAL S., 2010. *Geodetic measurements of vertical crustal velocity in West Antarctica and the implications for ice mass balance*, Geochem. Geophys. Geosyst., *10* (10), Q10005, doi:10.129/2009GC002642.

BOY J.-P., GEGOUT P. and HINDERER J., 2002. *Reduction of surface gravity data from global atmospheric pressure loading*, Geophys. J. Int., *149*, 534–545.

CROSSLEY D., HINDERER J., CASULA G., FRANCIS O., HSU H.-T., IMANISHI Y., JENTZSH G., KÄÄRIÄINEN J., MERRIAM J., MEURERS B., NEUMEYER J., RICHTER B., SHIBUYA K., SATO T., and VAN DAM T., 1999. *Network of superconducting gravimeters benefits a number of disciplines*, EOS. Am. Geophys. Union, *80* (11), 125–126.

DOWDESWELL J. A., BENHAM T. J., STROZZI T., and HAGEN J. O., 2008. *Iceberg calving flux and mass balance of the Austfonna ice cap on Nordaustlandet, Svalbard*, J. Geophys. Res., *113*, F03022, doi:10.1029/2007JF000905.

EKMAN M. and MÄKINEN J., 1996. *Recent postglacial rebound, gravity change and mantle flow in Fennoscandia*, Geophys. J. Int., *126*, 229–234.

FANG M. and HAGER B. H., 2001. *Vertical deformation and absolute gravity*, Geophys. J. Int., *146*, 539–548.

FARRELL W. E., 1972. *Deformation of the Earth by surface loads*, Rev. Geophys. Space Phys., *10*, 761–797.

HORWATH M. and DIETRICH R., 2009. *Signal and error in mass change inferences from GRACE: the case of Antarctica*, Geophys. J. Int., *177*, 849–864.

JAMES T. S. and IVINS E. R., 1998. *Predictions of Antarctic crustal motions driven by present-day ice sheet evolution and by isostatic memory of the last glacial maximum*, J. Geophys. Res., *103* (B3), 4993–5017.

KÄÄB A., 2008. *Glacier volume changes using ASTER satellite stereo and ICESat GLAS laser altimetry. A test study on Edgeøya, Eastern Svalbard*, IEEE Transactions on Geoscience and Remote Sensing, *46*, 10, 2823–2830.

KIERULF H. P., PLAG H.-P., and KOHLER J., 2009. *Surface deformation induced by present-day ice melting in Svalbard*, Geophys. J. Int., *179*, 1–13.

KOHLER J., JAMES T. D., MURRAY T., NUTH C., BRANDT O., BARRAND N. E., AAS H. F., and LUCKMAN A., 2007. *Acceleration in thinning rate on western Svalbard glaciers*, Geophys. Res. Lett., *34*, L18502, doi:10.1029/2007GL030681.

KORONA J., BERTHIER E., BERNARD M., REMY F., and THOUVENOT E., 2009. *SPIRIT. SPOT 5 stereoscopic survey of Polar Ice: Reference Images and Topographies during the fourth International Polar Year (2007–2009)*, ISPRS Journal of Photogrammetry and Remote Sens., *64*(2), 204–212.

LAMBERT A., COURTIER N., SASAGAWA G. S., KLOPPING F., WINESTER D., JAMES T. S., and LIARD J. O., 2001. *New constraints on Laurentide postglacial rebound from absolute gravity measurements*, Geophys. Res. Lett., *28*(10), 2109–2112.

LAMBERT A., COURTIER N., and JAMES T. S., 2006. *Long-term monitoring by absolute gravimetry: tides to postglacial rebound*, J. Geodyn., *43*, 339–357, doi:10.1016/j.jog.2006.08.002.

LARSON K. M. and VAN DAM T., 2000. *Measuring postglacial rebound with GPS and absolute gravity*, Geophys. Res. Lett., *27* (23), 3925–3928.

LE MEUR E. and HUYBRECHTS P., 2001. *A model computation of the temporal changes of surface gravity and geoidal signal induced by the evolving Greenland ice sheet*, Geophys. J. Int., *145*, 835–849.

DE LINAGE C., HINDERER J., and ROGISTER Y., 2007. *A search for the ratio between gravity variation and vertical displacement due to a surface load*, Geophys. J. Int., *171*, 986–994, doi:10.1111/j.1365-246X.2007.03613.x.

LUTHCKE S. B., ARENDT A. A., ROWLANDS D. D., MCCARTHY J. J., and LARSEN C. F., 2008. *Recent glaciers mass changes in the Gulf of Alaska region from GRACE mascon solutions*, J. Glaciol., *54* (188), 2109–2112.

MÄKINEN J., ENGFELDT A., HARSSON B. G., RUOTSALAINEN H., STRYKOWSKI G., OJA T., and WOLF D., 2005. *The Fennoscandian land uplift gravity lines 1966–2003*. In: Jekeli C., Bastos L., Fernandes J. (Eds), Gravity, Geoid and Space Missions–GGSM2004. IAG International Symposium. Porto, Portugal, August 30–September 3, 2004, IAG Symposia 129, Springer, pp. 328–332.

MÄKINEN J., AMALVICT M., SHIBUYA K., and FUKUDA Y, 2007. *Absolute gravimetry in Antarctica: status and prospects*, J. Geodyn., *41*, 307–317, doi:10.1016/j.jog.2005.08.032.

MÉMIN A., ROGISTER Y., HINDERER J., LLUBES M., BERTHIER E. and BOY J.-P., 2009. *Ground deformation and gravity variations modelled from present-day ice thinning in the vicinity of glaciers*, J. Geodyn., *48* (3–5), 195–203, doi:10.1016/j.jog.2009.09.006.

MÉMIN A., ROGISTER Y., HINDERER J., OMANG O. C. and LUCK B., 2011. *Secular gravity variation at Svalbard (Norway) from ground observations and GRACE satellite data*, Geophys. J. Int., *184*(3), 1119–1130, doi:10.1111/j.1365-246X.2010.04922.x.

MERRIAM J. B., 1992. *Atmospheric pressure and gravity*, Geophys. J. Int., *109*, 488–500.

MOHOLDT G., HAGEN J. O., EIKEN T., and SCHULER T. V., 2009. *Geometric changes and mass balance of the Austfonna ice cap, Svalbard*, The Cryosphere Discussions.

NUTH C., MOHOLDT G., KOHLER J., HAGEN J. O., and KÄÄB A., 2010. *Svalbard glacier elevation changes and contribution to sea level rise*, J. Geophys. Res., *115*, F01008,doi:10.1029/2008JF001223.

SATO T., OKUNO J., HINDERER J., MACMILLAN D. S., PLAG H. P., FRANCIS O., FALK R., and FUKUDA Y., 2006. *A geophysical interpretation of the secular displacement and gravity rates observed at , Svalbard in the Arctic–effects of post-glacial rebound and present-day ice melting*, Geophys. J. Int., *165*, 729–743.

SLOBBE D. C., DITMAR P. and LINDENBERGH R. C., 2009. *Estimating the rates of mass change, ice volume change and snow volume change in Greenland from ICESat and GRACE data*, Geophys. J. Int., *176*, 95–106.

TUSHINGHAM A.M. and PELTIER W.R., 1991. *ICE-3G: a new global model of Late Pleistocene deglaciation based upon geophysical predictions of postglacial relative sea level change*, J. Geophys. Res., *96*, 4497–4523.

VELICOGNA I., 2009. *Increasing rates of ice mass loss from the Greenland and Antarctic ice sheets revealed by GRACE*, Geophys. Res. Lett., *36*, L19503, doi:10.1029/2009GL040222.

WAHR J., DAZHONG H., and TRUPIN A., 1995. *Predictions of vertical uplift caused by changing polar ice volumes on a viscoelastic earth*, Geophys. Res. Lett., *22* (8), 977–980.

WOLF D., BARTHELMES F., and SIGMUNDSSON F., 1997. *Predictions of deformation and gravity variation caused by recent change of*

Vatnajökull ice cap, Iceland, Compt. Rend. J. Luxemb. Geodyn., *82*, 36–42.

WOUTERS B., CHAMBERS D., and SCHRAMA E. J. O., 2008. *GRACE observes small-scales mass loss in Greenland*, Geophys. Res. Lett., *35*, L20501, doi:10.1029/2008GL034816.